Section 1
PROGRESS IN LASER FUSION

1.A Results of Imploding-Target Burnthrough Experiments Using SSD Smoothing

Illumination uniformity is important for the success of inertial confinement fusion (ICF).[1] One potentially serious consequence of drive nonuniformity in direct-drive ICF experiments is the development of the Rayleigh-Taylor (RT) instability,[2] which can adversely affect target performance through mixing. Such mixing was assumed to be responsible for the discrepancy between the experimental and simulation results of the burnthrough experiments reported in Ref. 3. In those experiments, the laser irradiated a spherical target that consisted of a glass shell or a solid glass sphere overcoated with a parylene [or polyparaxylylene, $(CH)_x$] layer, in which one or more thin signature layers of moderate- to high-Z material were embedded for diagnostic purposes to signal the penetration of the heat front. Two potential regions for growth of the RT instability exist in such targets, one at the ablation surface and one at the parylene-signature-layer interface. Under current laser conditions, the instability grows from initial perturbations created mainly by the laser illumination nonuniformity, although normal target fabrication imperfections also play a minor role in initializing the instability. As laser uniformity improvements continue to be made, the contribution of these target imperfections will become more significant.

A primary result of the analysis in Ref. 3 was that the timing of the burnthrough was correlated with the illumination nonuniformity. This is based on the conclusion that mixing from a rapidly growing unstable region leads to an early burnthrough time. For similar shell drive conditions

(acceleration, mass-density scale length, and Atwood number), the RT growth rates should be similar and the rms amplitude of the instability should depend on the initial perturbation as long as the instability has not saturated. Thus, a conclusion of Ref. 3 was that the effectiveness of new methods developed to improve the laser illumination could be tested by measuring the burnthrough time in burnthrough targets, along with other observables affected by mixing, such as neutron yield and fuel density.

Since the data presented in Ref. 3 were collected, a number of improvements to the 351-nm irradiation uniformity of the 24-beam OMEGA laser have been implemented, including the use of distributed phase plates (DPP's)[4,5] and of smoothing by spectral dispersion (SSD).[6] In the SSD technique currently installed on OMEGA, a spectrally dispersed, broad-bandwidth, phase-modulated laser pulse is produced by an electro-optic phase modulator and a pair of transmission gratings, as shown in Fig. 48.1. When this pulse is focused onto the target through a DPP and a lens, the instantaneous speckle pattern formed on target by the DPP will vary rapidly as the red- and blue-shifted components cycle across the beam, resulting in an extremely uniform, time-averaged, far-field profile. The larger the bandwidth, the more rapidly the structure changes in time and achieves a given level of smoothing. This is illustrated in Figs. 48.2(a) and 48.2(b) where we have plotted the predicted rms on-target nonuniformity for various ℓ-mode ranges as a function of averaging time for two different bandwidths: $\Delta\lambda/\lambda = 5 \times 10^{-5}$ and $\Delta\lambda/\lambda = 3 \times 10^{-4}$. The initial ℓ-mode spectrum was the same in each case and was derived from measured-beam, far-field profiles. The effect of thermal smoothing has been included by multiplying the amplitude of each ℓ-mode by a factor $\exp(-0.01\ell)$, in accordance with the

Fig. 48.1
A schematic of SSD as implemented on the OMEGA laser system. A spectrally dispersed broad-bandwidth, phase-modulated pulse is produced by the electro-optic modulator and the pair of transmission gratings. R and B refer to the red- and blue-shifted components of the beam.

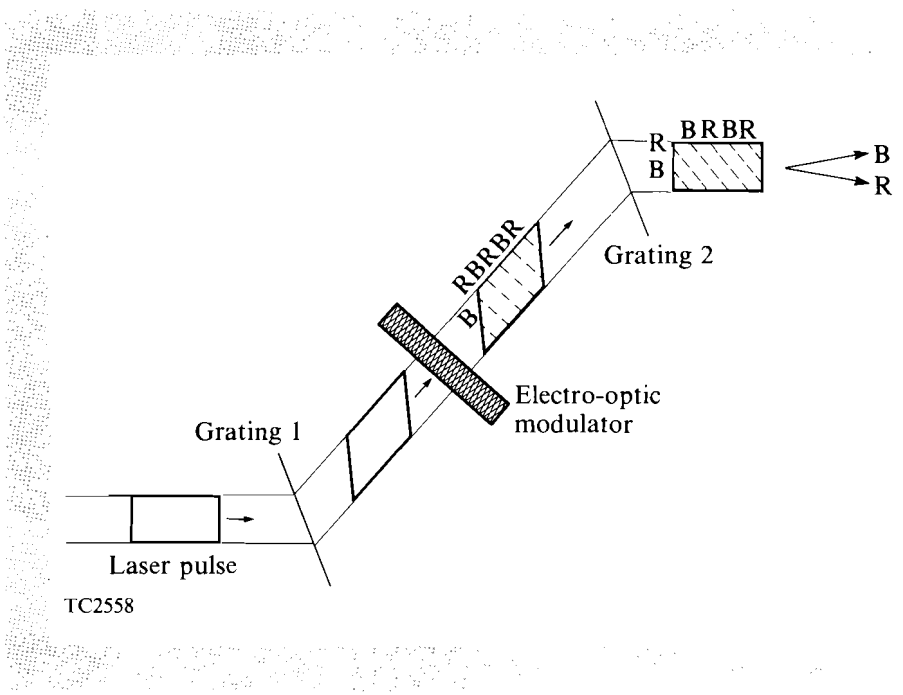

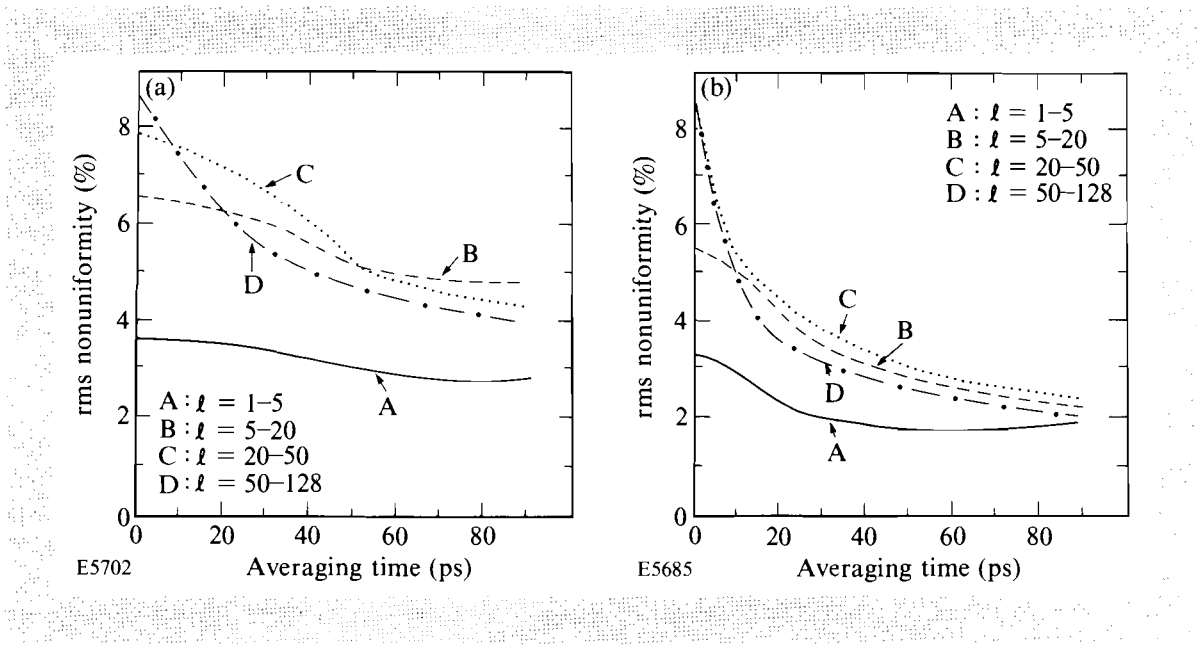

Fig. 48.2
Illumination rms nonuniformity on target for various ℓ-mode ranges as a function of averaging time for SSD bandwidths of (a) $\Delta\lambda/\lambda = 5 \times 10^{-5}$ and (b) $\Delta\lambda/\lambda = 3 \times 10^{-4}$. The modulation frequency was 8 GHz. In each case a thermal smoothing factor of 1% was assumed.

"cloudy-day" model.[7] By comparing the two figures it can be seen that the overall level of nonuniformity is expected to fall more quickly and to a lower asymptotic value in the higher bandwidth case than in the lower. It is also noteworthy that this effect is much more pronounced for the higher ℓ-modes, which are predicted to be the more destructive ones in terms of causing early burnthrough.[3]

In this article, we present results of burnthrough experiments undertaken to study the effect of the SSD bandwidth on both the burnthrough time and on the neutron yield of D_2-filled imploding targets. We observe that increasing the SSD bandwidth from zero to $\Delta\lambda/\lambda = 4 \times 10^{-4}$ increases the burnthrough time by about 200 ps. Based on simulations carried out on the one-dimensional (1-D) code *LILAC* and a mixing model postprocessor, we attribute these improvements to a decrease, as a result of SSD, in the amplitude of the initial perturbations that seed the RT instability.

The experiments were carried out on the OMEGA laser system at 351 nm with 600-ps FWHM Gaussian pulses at peak intensities of about $8–9 \times 10^{14}$ W/cm^2. DPP's were used throughout the experiment along with values for the SSD bandwidth ranging from $\Delta\lambda/\lambda = 0–4 \times 10^{-4}$. In all cases the SSD modulation frequency was 8.74 GHz. The targets consisted of 3-μm-thick glass shells with diameters ranging from 260 μm to 270 μm, filled with

50 atm of D_2 and coated with 6 μm of parylene. The parylene layer was chosen to be slightly larger than the computed 1-D burnthrough depth in order to give maximum sensitivity to changes in drive uniformity. A barrier layer, consisting of 0.1 μm of Al, was deposited on the targets to prevent shinethrough[8] of the early part of the laser pulse into the target before formation of the critical surface. X-ray emission from the barrier layers also served as a timing marker since a fiducial beam was not available for these experiments. Illumination uniformity and absorption were optimized by choosing targets with diameters about a factor of 1.28 smaller than the diameter of the first zero of the DPP point spread function (387 μm). Targets with such diameters intercept 81.5% of the beam energy.

Measurements of the temporal emission of the Al and Si H-like and He-like lines were provided by SPEAXS,[9] a time-resolving x-ray spectrometer in which an elliptically curved pentaerythritol (PET) crystal analyzer is used to disperse the x-ray spectrum (1.5- to 2.5-keV range) onto the slit of an x-ray streak camera. Neutron yields from the DD fusion reactions were measured using silver activation and a set of scintillator/photomultiplier pairs.[10,11] Figure 48.3 shows a typical SPEAXS spectrum containing K-shell emission from both the Al barrier layer and the glass signature layer. Lineouts along the time axis for both the Al and Si H-like 1s–3p lines are shown in Fig. 48.4. In view of the lack of an absolute laser timing fiducial

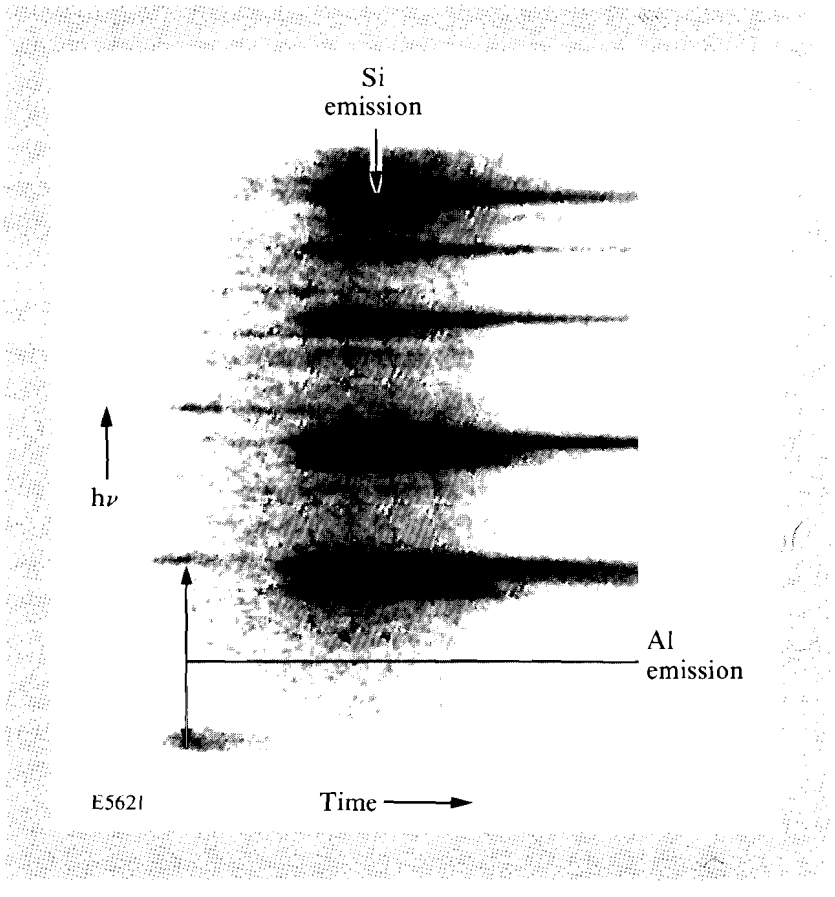

Fig. 48.3
Typical SPEAXS spectrum showing emission from both the outer Al layer and the glass signature layer (Si emission).

during these experiments and since for the purposes of this article we are only interested in relative measurements, we have defined the burnthrough time as the temporal difference between the onset of the Al and Si emission. (The onset is defined as the time at which the emission reaches 1/10 of its maximum value.) Data recorded on previous experiments, when a timing fiducial was present, would indicate that the Al onset time is ~600 ps before the peak of the laser pulse.

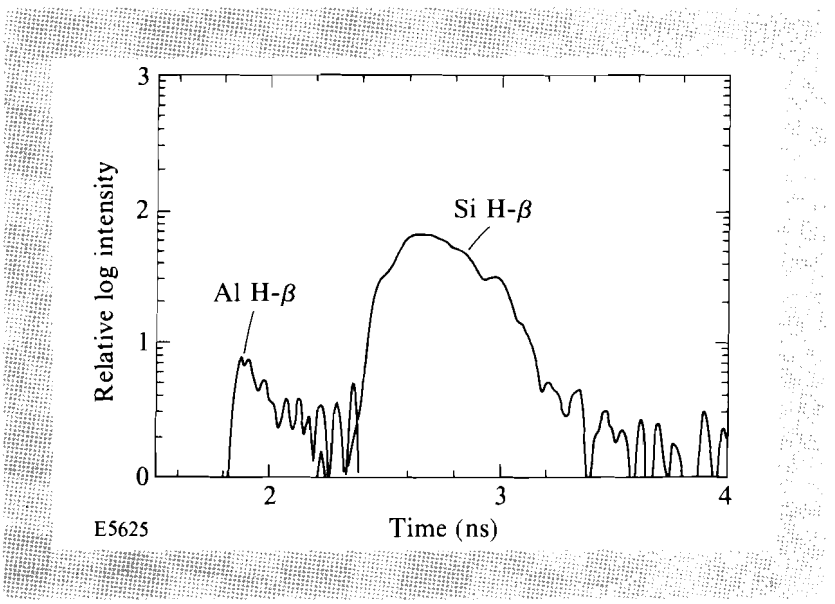

Fig. 48.4
Temporal lineouts of the Al and Si H-like 1s–3p lines. The choice of the zero point on the time axis is arbitrary.

Figure 48.5 shows the measured relative burnthrough times for several series of target shots with SSD bandwidths ranging from $\Delta\lambda/\lambda = 0\text{–}4\times 10^{-4}$. For the purposes of comparing data from several different shot series on the same graph, each with slightly different initial conditions, the burnthrough time at zero bandwidth has been defined as 0 ps for each series. Actual zero bandwidth time delays were typically ~550 ps between Al and Si emission, i.e., Si onset times were typically ~50 ps before peak laser power. There are two things to note from Fig. 48.5: (a) for all shot series we have always seen an improvement in burnthrough time when SSD bandwidth is present, compared to zero bandwidth shots, and (b) the burnthrough times continue to improve as SSD bandwidth is increased, with up to a 200-ps improvement at the maximum measured bandwidth of 4×10^{-4}. Figure 48.6 shows the measured neutron yield, expressed as a fraction of the 1-D yield predicted by *LILAC*, as a function of SSD bandwidth. In this case there is still a noticeable and consistent improvement when bandwidth is present, compared to shots without SSD. However, there is not as clear a trend of improving yield with increasing bandwidth as with the burnthrough times, indicating that the neutron yield is not as sensitive an indicator of illumination uniformity as the burnthrough measurement. This is consistent with the idea that, whereas the burnthrough time is sensitive to instabilities that develop during the acceleration phase of the implosion, the neutron yield, which occurs much later during the implosion, has the potential to be affected by many more physical

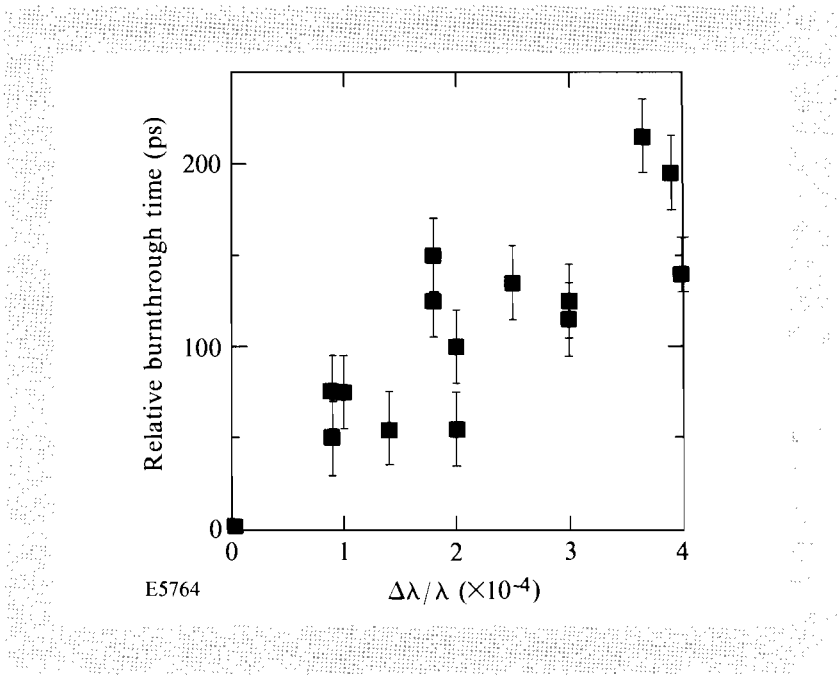

Fig. 48.5
Relative burnthrough times plotted as a function of SSD bandwidth. For each sequence of shots the zero-bandwidth case has been normalized to 0 ps to allow a comparison to be made.

processes, including additional fluid instabilities that can develop during the deceleration phase. Even at a bandwidth of 4×10^{-4} we still observe burnthrough into the glass layer shortly after the peak of the laser pulse, indicating that a substantial degree of mix has already occurred.

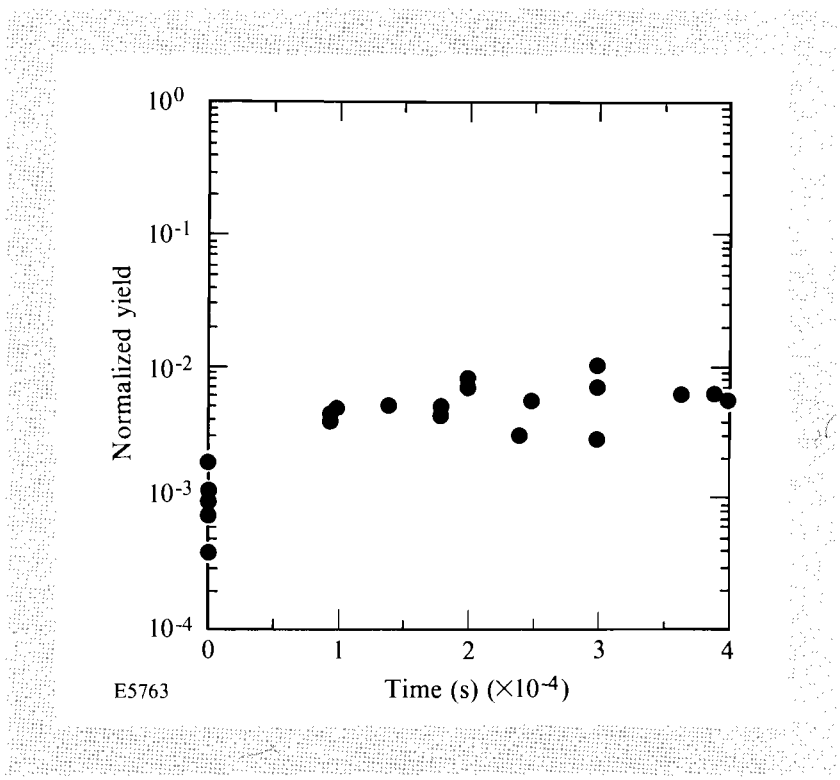

Fig. 48.6
Normalized neutron yields for the data in Fig. 48.5 plotted as a function of SSD bandwidth. The normalized yield is expressed in terms of the ratio of the measured yield to the 1-D yield predicted by *LILAC*.

The effect of SSD on the burnthrough time can be analyzed theoretically with the 1-D hydrodynamic code *LILAC* and a post-processor that models the evolution of the RT instability[3] and calculates a mixing thickness. For targets consisting of a parylene-coated glass shell we need to consider only the RT growth at the ablation surface. The growth rate at the glass-parylene interface is smaller than at the ablation surface because of the low Atwood number.[3] Burnthrough time is defined in the model as the time at which the mixing thickness is larger than the distance between the 200-eV isotherm and the glass-parylene interface. The mix thickness is calculated using a multi-mode analysis[12] in which each mode of an initial perturbation spectrum is evolved exponentially with a given growth rate. The analysis also includes a saturation model. The growth rate for the ablation-surface instability is stabilized by the ablation process and is expressed as[13] $\gamma = \alpha\sqrt{ka} - \beta k V_a$, where k is the unstable mode wave number, a is the acceleration, and V_a is the ablation velocity. The constant values $\alpha = 0.9$ and $\beta = 3$–4 provide a good fit to the growth rates obtained from full two-dimensional simulations. Further details on the model can be found in Ref. 3.

The main effect of SSD is to modify the initial perturbation spectrum. As can be seen from Fig. 48.2, SSD reduces the smoothing time and also smooths out the higher ℓ-modes faster and more efficiently than the lower ℓ-modes. The temporal effect of SSD is too complex to be included into the mix model. Instead, we will show that the reduction of the higher ℓ-mode amplitude in the initial perturbation spectrum leads to a reduction in the mix thickness, which in turn increases the burnthrough time. In Fig. 48.2 the rms perturbation is given as a percentage of the beam laser energy on target. The mixing post-processor, however, requires an initial perturbation of the target surface. We have at this point no way to calculate either the rms surface perturbations from a given illumination rms perturbation or the surface perturbation that will yield the hydrodynamic behavior equivalent to a given illumination perturbation. For the purpose of this article we assume that the illumination perturbation produces an equivalent surface perturbation, or at least, that the surface perturbation is proportional to the illumination perturbation. A more complex relationship between the illumination perturbation and the surface perturbation would only change the parameters in the initial perturbation spectrum, but not the conclusion of the analysis.

Initial perturbation spectra for the zero-bandwidth case and the maximum-bandwidth case were constructed partly from a sum of two exponential functions so as to approximate the measured irradiation uniformity on target.[14] The published spectra were generated only to $\ell = 64$. The constructed spectra are given by $A_{\ell,m}(t=0) = \xi_0[\exp(-S_1\ell) + R_2 \exp(-S_2\ell)]$ (μm/mode) and $A_{\ell,m} = A_{35,m}$ for $35 < \ell < 64$, where ξ_0 is the initial perturbation in μm, ℓ is the Legendre mode number, S_1 and S_2 are chosen to obtain the required rms nonuniformity, and $R_2 = \exp[(S_2 - S_1)\ell_0]$, with ℓ_0 set for a given spectrum. This formalism provides flexibility and a description of the initial perturbation that depends on one parameter ξ_0. (The modes are assumed to be symmetric in the azimuthal direction.) Appropriate values for S_1, S_2, and ℓ_0 are, for zero bandwidth, $S_1 = 0.13$, $S_2 = -0.039$, and $\ell_0 = 17$;

for full bandwidth, $S_1 = 0.20$, $S_2 = 0.0$, and $\ell_0 = 17$. The constructed spectra need to be extended to $\ell = 200$ in order to include the fastest growing modes near $\ell = 100$. Assuming the same 1% thermal smoothing by the target as in Fig. 48.2, the extended spectra were given the form $\exp(-0.01\ell)$ for $64 < \ell < 200$. Figure 48.7 shows the constructed initial spectrum for the zero-bandwidth (curve a) and the full-bandwidth (curve b) cases for the same initial amplitude ξ_0. The effect of SSD is to reduce the rms nonuniformity mainly for modes above about $\ell = 10$.

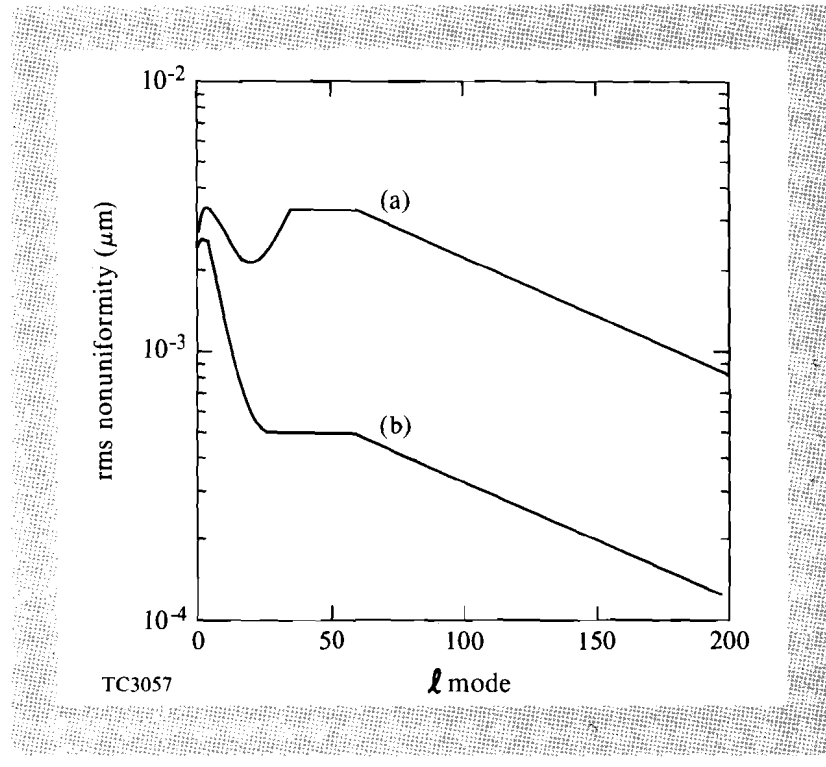

Fig. 48.7
ℓ-mode distribution of the initial perturbation used in the model to estimate the mixing-region thickness. Curve (a) is for zero bandwidth and curve (b) is for the maximum bandwidth case ($\Delta\lambda/\lambda = 4 \times 10^{-4}$).

The value of ξ_0 is chosen such that the computed delay between the onset of the Si and Al emission is approximately equal to the measured time delay for the zero-bandwidth case. Because of the lack of a timing fiducial in the measurements, a comparison of absolute burnthrough times between the experiment and the simulation is not possible. Also, the resonance line emission from the Al barrier layer cannot be used for a precise timing comparison because the computed temporal emission from *LILAC* depends on the laser pulse shape early in time, which is not known accurately. Since we want to show only the relative effect of decreasing the initial perturbation, an absolute timing comparison is not necessary; however, the computed burnthrough times still need to be realistic in order to make the argument credible. Based on previous measurements of the Al barrier-layer emission in which a timing fiducial was present, we assume that the Al emission occurs 600 ps before the peak of the pulse.

The effect of SSD on the burnthrough times can be observed in simulations of the targets previously described. Using the zero-bandwidth spectrum

in Fig. 48.7 (curve a), a value for $\xi_0 = 350$ Å gives a burnthrough time of about −65 ps with respect to the peak of the laser pulse, approximately the time measured in the experiment. Using the maximum-bandwidth spectrum in Fig. 48.7 (curve b) and the same value for ξ_0 gives a burnthrough time of +95 ps. Thus, when SSD is added to the mix model, keeping the initial perturbation amplitude constant, the burnthrough time is advanced by 160 ps. This value agrees reasonably well with the 200-ps time delay between the zero-bandwidth and the maximum-bandwidth burnthrough times measured in the experiment. Therefore, within the limitations of modeling the initial perturbation in the mix model, we have shown that improving the illumination uniformity with SSD in the mix model, through the reduction in the amplitude of modes $\ell > 10$, accounts for the observed increase in the burnthrough time. Also, the analysis confirms that the evolution of the instability remains mostly linear as defined in Ref. 12.

In summary, we have investigated the effect of the drive-uniformity improvements resulting from SSD in burnthrough experiments. We had shown in previous work that the burnthrough time is a measure of the evolution of the RT instability at the ablation surface and the glass-parylene interface. Since the evolution does not saturate it depends on the initial perturbation and should, therefore, be sensitive to the level of illumination nonuniformity. The measured burnthrough times show continued improvement as the SSD bandwidth is increased from zero to $\Delta\lambda/\lambda = 4 \times 10^{-4}$, consistent with a continually improving uniformity. The neutron yields show an immediate improvement with a small amount of SSD bandwidth present, but do not show a strong bandwidth dependence beyond that. The measured improvements in burnthrough times can be reproduced by a post-processor to the 1-D code *LILAC* that models the evolution of the RT instability and includes initial perturbation spectra consistent with the measured change in uniformity.

ACKNOWLEDGMENT

The authors would like to thank S. Skupsky for providing the irradiation uniformity data and for many useful discussions, the target fabrication group, and the members of the OMEGA laser and experimental operations groups. This work was supported by the U.S. Department of Energy Office of Inertial Confinement Fusion under agreement No. DE-FC03-85DP40200 and by the Laser Fusion Feasibility Project at the Laboratory for Laser Energetics, which is sponsored by the New York State Energy Research and Development Authority and the University of Rochester.

REFERENCES

1. J. Nuckolls *et al.*, *Nature* **239**, 139 (1972).
2. S. Chandrasekhar, *Hydrodynamic and Hydromagnetic Stability* (Clarendon Press, Oxford, England, 1961), Chap. 10.
3. J. Delettrez, D. K. Bradley, P. A. Jaanimagi, and C. P. Verdon, *Phys. Rev. A* **41**, 5583 (1990).
4. Y. Kato *et al.*, *Phys. Rev. Lett.* **53**, 1057 (1984).
5. LLE Review **33**, 1 (1987).